Nutr Cycl Agroecosyst (2014) 100:189–204
DOI 10.1007/s10705-014-9637-6

ORIGINAL ARTICLE

A new slurry pH model accounting for effects of ammonia and carbon dioxide volatilization on solution speciation

V. Petersen · R. Markfoged · S. D. Hafner · S. G. Sommer

Received: 25 March 2014 / Accepted: 22 August 2014 / Published online: 2 September 2014

Abstract Ammonia (NH_3) emissions from manure constitute a significant loss of fixed nitrogen (N) from agricultural systems and contribute to air pollution and ecosystem degradation. Accurate models of such NH_3 emissions will improve our understanding of the factors that control the emissions and allow appropriate mitigation actions to be identified and quantified. Although the importance of manure pH on ammonia emission has been recognized for decades, the physical and chemical interactions that control pH are not fully understood. Here we present a novel mathematical model that includes the dynamic and crucial pH changes in the surface of stored slurry or slurry applied in the field. In the model, slurry pH is calculated by simultaneously determining: (1) speciation of the acid–base reactions, (2) diffusion of each buffer species, and (3) emission of NH_3 and CO_2. New features of the model include a reduced variable that combines time and location and an analytical approach to solving the resulting system of equations using Mathematica. To evaluate the model, we made measurements of pH at a resolution of 0.1 mm in the top 30 mm of an ammonium bicarbonate solution. These measurements show the creation of a large pH gradient (>1 pH unit in <30 mm after 20 h) and its change over time due to simultaneous NH_3 and CO_2 emission from aqueous solutions. The model was able to accurately predict the development of pH gradients over time, suggesting that our understanding of the factors controlling pH is correct. New developments presented in the model should be useful for future work on understanding and predicting NH_3 emission from manure.

Keywords Ammonia · pH · Carbon dioxide · Emission model · Manure slurry

Abbreviations

D_X	Diffusion coefficient of chemical species X in water ($cm^2\ s^{-1}$)
$D_{X,Air}$	Diffusion coefficient of chemical species X in air ($cm^2\ s^{-1}$)
F_X	Constant determining how quickly the species X is transported from water to air through the water–air surface ($mol\ L^{-1}\ cm\ s^{-1/2}$). The cumulative mass transported to the air through area A over time t is given by the expression $A\sqrt{t}F_x$

Electronic supplementary material The online version of this article (doi:10.1007/s10705-014-9637-6) contains supplementary material, which is available to authorized users.

V. Petersen · S. D. Hafner (✉) · S. G. Sommer
Faculty of Engineering, Institute of Chemical Engineering, Biotechnology and Environmental Engineering, University of Southern Denmark (SDU), Odense M, Denmark
e-mail: saha@kbm.sdu.dk

R. Markfoged
Department of Bioscience, Microbiology, Aarhus University, Aarhus, Denmark

$H_X = \frac{[X]_0}{[X]_{0,Air}}$	Henrýs law constant for the chemical species X (dimensionless)
K_X	Equilibrium constant for the chemical reaction of the species X
z	Depth in solution or height in the air, always positive (cm)
t	Time since stirring, always positive (s)
$w = \frac{z}{\sqrt{t}}$	Reduced variable, always positive (cm $s^{-1/2}$)
$[X]$	Concentration of chemical species X in water (mol L^{-1})
$[X]_{Air}$	Concentration of chemical species X in air (mol L^{-1})
$[X]_0$	Concentration of chemical species X in water at the water–air surface (mol L^{-1})
$[X]_\infty$	Concentration of chemical species X in water at infinite depth (bulk value) (mol L^{-1})
$[X]_{0,Air}$	Concentration of chemical species X in air at the water–air surface (mol L^{-1})
$[X]_{\infty,Air}$	Concentration of chemical species X in air at infinite height (bulk value) (mol L^{-1})
TAN	Total Ammonia Nitrogen: $[TAN] = [NH_3] + [NH_4^+]$ (mol L^{-1})
TIC	Total Inorganic Carbon: $[TIC] = [CO_2] + [HCO_3^-] + [CO_3^{-2}]$ (mol L^{-1})
α_x	Ionization fraction for TAN or TIC: $[X] = \alpha_x[TAN]$ or $[X] = \alpha_x[TIC]$. It is a polynomial fraction which depends only on $[H_3O^+]$ and has values between 0 and 1 (dimensionless)

Introduction

Emissions of ammonia (NH_3) from livestock waste or manure represent a loss of valuable plant nutrients, a source of air pollution and a threat to terrestrial and aquatic ecosystems (Galloway et al. 2003; Sutton et al. 2011). Indirectly, NH_3 deposition also contributes to nitrous oxide (N_2O) emissions by increasing N cycling in natural ecosystems (Davidson 2009). There is global consensus that agriculture, in particular livestock manure, is a large source of NH_3 emissions to the atmosphere (Beusen et al. 2008). The sources of this NH_3 are livestock manure in animal houses, stored manure and manure applied in the field.

Ammonia emissions are an environmental problem and researchers and regulators need knowledge on the NH_3 emission rate in order to assess NH_3 deposition in ecosystems and develop measures to reduce emissions. Such measures are specified by the UN in its Convention on Long-Range Transboundary Air Pollution (CLRTAP), in the Gothenburg Protocol (United Nations 2004) and in the EU National Emissions Ceilings (NEC) Directive (EU 2001). Ammonia emissions also represent a loss of fixed N and contribute to inaccuracy in knowledge about the amount of fixed N available for plant production, reducing the precision of predicted plant nutrient requirements in the field. Thus national authorities and farmers require reliable models that precisely predict NH_3 emissions from specific manure management systems and livestock production practices.

Various models for calculating NH_3 emissions have been developed. These models range in complexity from static emission factors (Buijsman et al. 1987; Hutchings et al. 2001) to dynamic physical and chemical models (van der Molen et al. 1990; Génermont and Cellier 1997; Ni 1999). A challenge for all models for NH_3 emission from manure is accurate representation of the interactions between carbon dioxide (CO_2) and NH_3 emission and slurry pH, which is the focus on the current work. While it has been known for decades that slurry pH affects NH_3 emission rate, recent work has highlighted the complexity of this interaction. The pH in the liquid layer close to the exposed surface may be significantly different from that in the bulk of the source due to emission of CO_2 and NH_3 (Sommer and Sherlock 1996; Canh et al. 1998). Model predictions and limited measurements suggest that the resulting pH gradient substantially affects NH_3 emission, and is itself influenced by manure composition and environmental properties (Chaoui et al. 2009; Blanes-Vidal et al. 2009; Hafner et al. 2013). Understanding this effect is particularly important for predicting NH_3 emission because pH has a large effect on free ammonia concentration and therefore emission rate. For example, at 15 °C, typical dairy slurry with a total ammonia N (TAN, $TAN = NH_3 + NH_4^+$) concentration of 1.5 g/L has 12 mg/L (as N) of free NH_3 at pH 7.5. Free NH_3 increases to 115 mg N/L as the pH increases to 8.5 [based on Eq. (12) in Hafner and Bisogni (2009), and following Hafner et al. (2013) for activity coefficients]. While experimental approaches can be

useful for developing and evaluating methods for reducing NH_3 emission, empirical results are limited to specific conditions and cannot provide truly predictive tools. Furthermore, a thorough understanding of the processes involved in ammonia emission may lead to new insights for controlling emission. It is with this perspective that the current work focuses on developing a better understanding of interactions controlling manure pH.

Because of the complexity of manure, this current work focuses on simpler solutions of ammonium bicarbonate (NH_4HCO_3). This focus is necessary for understanding the importance of interactions between CO_2 and NH_3 emission and pH. It is not our goal here to develop a comprehensive model for NH_3 emission from manure that includes all possible processes, although this current work could inform such an effort. In the last 5 years, mathematical models have shown that CO_2 emission significantly affects the pH and rate of NH_3 emission (Blanes-Vidal et al. 2009; Hafner et al. 2013). This earlier work has some limitations, and, perhaps more importantly, model evaluation has been very limited. Blanes-Vidal et al. (2009) used a relatively simple two-film model that used linear concentration profiles for chemical species and assumed the mass of NH_3 within the liquid film was negligible for NH_3 emission. These assumptions are not valid for the dynamic conditions that exist in field-applied manure. Hafner et al. (2013) presented a more sophisticated dynamic model that included equilibrium and kinetically limited reactions. But this model was numeric, and so cannot as easily provide the generalizations and insights that can be gained from an analytical approach. Existing model evaluation has been limited to NH_3 emission measurements and a small number of pH measurements from simple solutions reported in Hafner et al. (2013). Measurements of pH in manure suggest that some increase in surface pH does occur when manure is exposed to air (Bussink et al. 1994; Chaoui et al. 2009). Together, these measurements provide evidence that the predictions made by Hafner et al. (2013) are correct, but to date no measurements have clearly shown the large gradients in pH predicted to exist near the surface. The objectives of the current work were to: (1) develop an analytical model for simultaneous emission of CO_2 and NH_3 from NH_4HCO_3 solutions, including prediction of pH over space and time, and (2) evaluate the model with high-resolution measurements of pH near the surface of a solution in the laboratory. This work presents a new mathematical model that introduces two important developments: incorporation of a reduced variable that incorporates time and space and an analytical approach to model implementation using the software *Mathematica*. Additionally, this work is the first to report measurements of pH in an ammonium bicarbonate solution at a fine spatial resolution (0.1 mm) over time as NH_3 and CO_2 volatilize. Lastly, measurements are used to evaluate model predictions, and the model is used to quantify the effects of changes in gas- and liquid-phase resistance.

Methods

Model description

Manure is a mixture of many solutes, but the most important buffer components are TAN and inorganic carbon. The model includes these components and also K^+ and Cl^-. For an NH_4HCO_3 solution, the uncharged gas species NH_3 and CO_2 are released to the atmosphere. The volatilization of NH_3 from the liquid is dependent on the relationship between concentration or partial pressure of NH_3 in the air and concentration of NH_3 in the liquid surface (Fig. 1). Ammonia is a base with the conjugating acid being ammonium (NH_4^+), and so the ratio of NH_3 to NH_4^+ is controlled by the H_3O^+ concentration. In an NH_4HCO_3 solution, the H_3O^+ concentration is related to the concentration of pH buffers present as total inorganic carbon ($TIC = CO_2 + HCO_3^- + CO_3^{-2}$) and TAN. Carbon dioxide emission from the surface of a source of NH_4HCO_3 decreases the H_3O^+ concentration [H_3O^+], while NH_3 emission increases it. The solubility of CO_2 is much less than that of NH_3, and hence CO_2 is initially emitted more rapidly than NH_3 from most slurries and the H_3O^+ concentration is generally less near the surface than in the bulk solution.

Emission of CO_2 and NH_3 from the surface of the source reduces the concentration of TIC and TAN species in the surface layer, and triggers upward diffusional transport of these from the layers below. Calculations of the H_3O^+ concentration in the surface layer must therefore include diffusive transport of TAN and pH buffer components to the surface, as well as emission of CO_2 and NH_3.

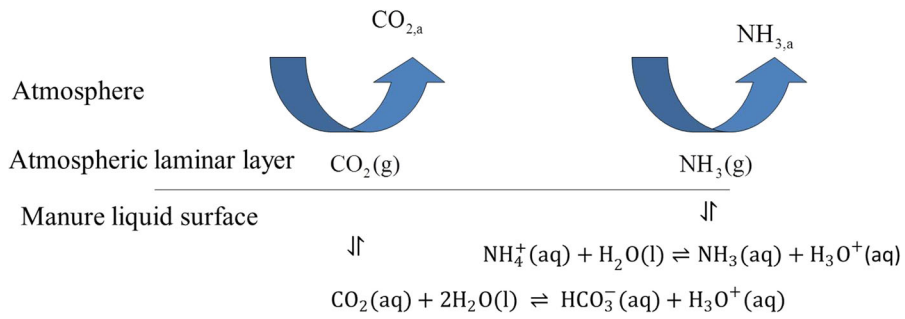

Fig. 1 The processes included in our model. Emission of NH_3 increase the H_3O^+ concentration, while emission of CO_2 decrease H_3O^+ concentration. Changes in the speciation of TAN and TIC affect their diffusive transport in the laminar undisturbed surface layers. The resulting changes in the concentration of TAN and TIC alter the H_3O^+ concentration

In this study, a model that includes equilibrium reactions of the TIC and TAN species was developed. The model calculates both diffusive transport of each species to the surface and the change in H_3O^+ concentration as affected by diffusion and volatilization of CO_2 and NH_3. The model assumes that; (1) the liquid is infinitely deep (i.e., sufficiently deep that volatilisation of CO_2 and NH_3 do not affect the composition of the deepest layers), (2) transport of gases and ions are controlled by diffusion (transport due to convection is not included), (3) acid–base reactions are rapid in relation to diffusion and are assumed to attain chemical equilibrium instantaneously, and (4) the solution is homogeneous at the start, and the same applies to the ambient atmosphere. The ambient concentration of gaseous NH_3 is considered to be zero.

Chemical reactions

The important components in the system of volatile buffer components significantly affecting NH_3 volatilisation are TAN and TIC (Sommer and Husted 1995), and the aqueous solution is composed of the following species: NH_3, NH_4^+, CO_2, HCO_3^-, CO_3^{2-}, H_3O^+, OH^-, K^+ and Cl^-. In the model, we ignored slow CO_2 hydration/dehydration reactions because the carbonic anhydrase added to the solution speeds up the reaction converting carbonic acid (H_2CO_3) to CO_2 and H_2O. Carbonic acid was considered to be part of the aqueous CO_2, which was assumed to be in equilibrium with HCO_3^- and CO_3^{-2}. The chemical reactions taking place in the solution are as follows:

$$NH_3 + H_2O \rightleftharpoons NH_4^+ + OH^-, K_{NH_3} \quad (1)$$

$$CO_2 + 2H_2O \rightleftharpoons HCO_3^- + H_3O^+, K_{CO_2} \quad (2)$$

$$HCO_3^- + H_2O \rightleftharpoons CO_3^{-2} + H_3O^+, K_{HCO_3^-} \quad (3)$$

$$2H_2O \rightleftharpoons H_3O^+ + OH^-, K_{H_2O} \quad (4)$$

$$[TAN] = [NH_3] + [NH_4^+] \quad (5)$$

$$[TIC] = [CO_2] + [HCO_3^-] + [CO_3^{2-}] \quad (6)$$

Equations for equilibrium constants are given in Table 1. Throughout, we use the mathematical tool *Mathematica* (Wolfram Research, Boston MA, USA) which can perform exact algebra, arbitrary precision computation and fast computation with standard floating point numbers.To implement our model, this tool was used to solve the Eqs. (1)–(6) for the six variables $[NH_3]$, $[NH_4^+]$, $[CO_2]$, $[HCO_3^-]$, $[CO_3^{-2}]$, and $[OH^-]$. In order to simplify the solutions, ionization fractions α_x are used (Annex A). The solutions to Eqs. (1)–(6) are then expressed as:

$$\begin{aligned} &[NH_3] = \alpha_{NH_3}[TAN],\ [NH_4^+] = \alpha_{NH_4^+}[TAN] \\ &[CO_2] = \alpha_{CO_2}[TIC],\ [HCO_3^-] = \alpha_{HCO_3^-}[TIC], \\ &[CO_3^{-2}] = \alpha_{CO_3^{-2}}[TIC] \\ &[OH^-] = K_{H_2O}/[H_3O^+] \end{aligned} \quad (7)$$

The ionization fractions α_X depend only on $[H_3O^+]$. They are simple polynomial fractions of the variable $[H_3O^+]$ and have values between 0 and 1. The sum of the two weight factors associated with TAN and the three weight factors associated with TIC are always 1.

Table 1 Dissociation constants of equilibria of TIC and TAN species and Henry's constants for CO_2 and NH_3 (Beutier and Renon 1978)

Reaction	Henry's constant H (dimensionless) and equilibrium constants K_C
$NH_3(g) \rightleftharpoons NH_3(aq)$	$H_{NH_3} = RT\exp[-(160.559 - 8621.06/T - 25.6767\ln(T) + 0.035388T)]$
$CO_2(g) \rightleftharpoons CO_2(aq)$	$H_{CO_2} = RT\exp[-(1082.37 - 34417.2/T - 182.28\ln(T) + 0.25159T)]$
$NH_3(aq) + H_2O(l) \rightleftharpoons NH_4^+(aq) + OH^-(aq)$	$K_{NH_3} = \exp[191.97 - 8451.61/T - 31.4335\ln(T) + 0.0152123T]$
$H_2O(l) \rightleftharpoons H^+(aq) + OH^-(aq)$	$K_{H_2O} = \exp[14.01708 - 10294.83/T - 0.039282T]$
$CO_2(aq) + H_2O(l) \rightleftharpoons HCO_3^-(aq) + H^+(aq)$	$K_{CO_2} = \exp[2767.92 - 80063.5/T - 478.653\ln(T) + 0.714984T]$
$HCO_3^-(aq) \rightleftharpoons CO_3^{2-}(aq) + H^+(aq)$	$K_{HCO_3} = \exp[12.405 - 6286.89/T - 0.050628T]$

T = temperature in K, R = universal gas constant = 0.082057 L atm/mol-K

The aqueous solution must be electrically neutral, and therefore the sum of charges of all the ions must be zero:

$$Z_{total} = [NH_4^+] + [H_3O^+] + [Na^+] - [HCO_3^-] - 2[CO_3^{-2}] - [OH^-] - [Cl^-] \quad (8)$$

Replacing the ion concentrations in Eq. (8) with the expressions from Eq. (7) reveals that Z_{total} depends linearly on [TAN] and [TIC] as a simple polynomial fractions of $[H_3O^+]$. Since [TAN] and [TIC] are positive, it can be shown mathematically that the equation $Z_{total} = 0$ has exactly one positive solution for $[H_3O^+]$. Consequently, $[H_3O^+]$ is a well-defined function of [TAN] and [TIC], and if [TAN] and [TIC] are known, the concentrations of all species in the solution are known. Annex B presents the arguments for this conclusion.

Diffusion and chemical reactions

The system described by the model represents an idealised environment where the liquid is infinitely deep and the air space is infinitely high. It is also assumed that the liquid and the air above the liquid are homogeneous initially, irrespective of depth/height z, and that all reactions in the liquid have reached chemical equilibrium. In this situation there is no net diffusion and no chemical reaction.

With time, the liquid system will deviate from chemical equilibrium due to the release of NH_3 and CO_2 from liquid to air through the liquid–air interface. Near the surface, this will result in chemical reactions seeking to establish a new equilibrium. As the concentration of each component is no longer constant in space, diffusion will also occur. With the passage of time, this change in concentration of species, which starts at the air–liquid surface, will move deeper into the liquid. A precise mathematical description of this change can be developed, as demonstrated below.

We assumed no convection in the liquid or air and consequently all transport of chemical species occurs through diffusion, both in the liquid and in air. We also assumed that chemical reactions are very fast compared with diffusion. These assumptions mean that there is a local chemical equilibrium at any time t and any depth z for all species at the point (t, z). Therefore, all expressions and Eqs. (1)–(8) and results derived from these apply to any point (t, z). As a consequence, the concentration of each species at the point (t, z) is a known function of [TAN] and [TIC] at this point. However, this function is only given by solving the equation $Z_{total} = 0$.

In a short time interval Δt at time t and depth z, changes in $[NH_3]$ and $\left[NH_4^+\right]$ are due to diffusion and chemical reactions. Therefore:

$$\Delta[NH_3] = \Delta[NH_3]_{diffusion} + \Delta[NH_3]_{reaction} \quad (9)$$

$$\Delta\left[NH_4^+\right] = \Delta\left[NH_4^+\right]_{diffusion} + \Delta\left[NH_4^+\right]_{reaction} \quad (10)$$

Fick's second law gives the change in concentration of component X due to diffusion as:

$$\Delta X = D\frac{\partial^2 X}{\partial z^2}\Delta t \quad (11)$$

where D is the diffusion coefficient of X in water. Adding Eqs. (9) and (10) and including Eq. (11) gives:

$$\Delta[NH_3] + \Delta[NH_4^+] = D_{NH_3}\frac{\partial^2[NH_3]}{\partial z^2}\Delta t + D_{NH_4^+}\frac{\partial^2[NH_4^+]}{\partial z^2}\Delta t + \Delta[NH_3]_{reaction} + \Delta[NH_4^+]_{reaction} \quad (12)$$

The left-hand side of Eq. (12) is equal to Δ[TAN] and $\Delta[NH_3]_{reaction} + \Delta[NH_4^+]_{reaction} = \Delta[TAN]_{reaction} = 0$.

Therefore, dividing by Δt and letting Δt progress towards zero gives the following differential equation:

$$\frac{\partial[TAN]}{\partial t} = D_{NH_3}\frac{\partial^2[NH_3]}{\partial z^2} + D_{NH_4^+}\frac{\partial^2[NH_4^+]}{\partial z^2} \quad (13)$$

Applying the weight factors [Eq. (7)] and introducing the following expression,

$$D_{TAN} = D_{NH_3}\alpha_{NH_3} + D_{NH_4^+}\alpha_{NH_4^+} \quad (14)$$

gives the fundamental partial differential equation for [TAN]:

$$\frac{\partial[TAN]}{\partial t} = \frac{\partial^2}{\partial z^2}(D_{TAN}[TAN]) \quad (15)$$

Following a similar argument, we get the partial differential equation for [TIC]:

$$\frac{\partial[TIC]}{\partial t} = \frac{\partial^2}{\partial z^2}(D_{TIC}[TIC]) \quad (16)$$

where:

$$D_{TIC} = D_{CO_2}\alpha_{CO_2} + D_{HCO_3^-}\alpha_{HCO_3^-} + D_{CO_3^{-2}}\alpha_{CO_3^{-2}} \quad (17)$$

D_{TAN} and D_{TIC} are known functions of $[H_3O^+]$ alone. Because of this dependence on $[H_3O^+]$ it should be noted that D_{TAN} and D_{TIC} are generally not constant and cannot be considered as diffusion coefficients. Calculation of diffusion coefficients was done using the equations given in Table 2.

If the two diffusion coefficients associated with [TAN] were identical, then D_{TAN} would be constant and have the value $D_{TAN} = D_{NH_3} = D_{NH_4^+}$, because $\alpha_{NH_3} + \alpha_{NH_4^+} = 1$. In this case the differential equation would thus be reduced to the ordinary diffusion equation $\frac{\partial[TAN]}{\partial t} = D_{TAN}\frac{\partial^2[TAN]}{\partial z^2}$. These arguments and results also apply to TIC. In a real system, the diffusion coefficients of the two TAN species are not identical and this also applies to the three TIC species. The two partial differential Eqs. (15) and (16) are therefore complicated and they are interconnected through D_{TAN} and D_{TIC}.

In a situation where all concentrations are initially constant, it will be shown that the concentrations in the solution depend only on t and z through the reduced variable $w = \frac{z}{\sqrt{t}}$. This simplification significantly reduces calculation work and time, since the problem is then one-dimensional instead of two-dimensional.

Table 2 Diffusion coefficients of TIC and TAN species (1: Zeebe 2011; 2: Frank et al. 1996; 3: Spiller 1989; 4: Marrero and Mason 1972)

Species	Diffusion coefficient ($cm^2\ s^{-1}$)	Ref
CO_2(aq)	$D_{CO_2} = 14.6836 \cdot 10^{-5}\left(\frac{T}{217.2056} - 1\right)^{1.9970}$	1
HCO_3^-(aq)	$D_{HCO_3^-} = 7.0158 \cdot 10^{-5} \cdot \left(\frac{T}{204.0282} - 1\right)^{2.3942}$	1
CO_3^{2-}(aq)	$D_{CO_3^{-2}} = 5.4468 \cdot 10^{-5} \cdot \left(\frac{T}{210.2646} - 1\right)^{2.1929}$	1
NH_3(aq)	$D_{NH_3} = 1.51 \cdot 10^{-5}\frac{T}{293}\frac{\mu_{293}}{\mu_T}$	2*
NH_4^+(aq)	$D_{NH_4^+} = 2.0 \cdot 10^{-5}\frac{T}{293}\frac{\mu_{293}}{\mu_T}$	2*
NH_3(g)	$D_{NH_3,Air} = 0.228 \cdot \left(\frac{T}{298.15}\right)^{1.5}$	3**
CO_2(g)	$D_{CO_2,Air} = 2.70 \cdot 10^{-5}T^{1.59} \cdot \exp\left(-\frac{102.1}{T}\right)$	4

* The temperature dependence for coefficients for NH_4^+ and NH_3 in water is a result of $D = D_0\frac{T}{T_0}\frac{\mu_0}{\mu}$ (Stokes–Einstein, Frank et al. 1996), where $\frac{\mu_T}{\mu_{293}} = 10^{\frac{293-T}{T-177}\left(1.2364-1.37\cdot10^{-3}\cdot(293-T)\right)}$ is the viscosity of water at temperature T (Kerstin et al. 1978), $D_{NH_3,293} = 1.51 \times 10^{-5}\ cm^2\ s^{-1}$ (Frank et al. 1996) and $D_{NH_4^+,293} = 2.0 \times 10^{-5}\ cm^2\ s^{-1}$ (Broboff et al. 1998)

** Temperature dependence of NH_3(g) diffusion is given by $D = D_0\left(\frac{T}{T_0}\right)^{3/2}$ (Chapman–Enskog)

By introducing the reduced variable w, the two partial differential Eqs. (15) and (16) are converted into the following two ordinary differential equations:

$$\frac{1}{2}w\frac{d}{dw}[TAN] + \frac{d^2}{dw^2}(D_{TAN}[TAN]) = 0 \quad (18)$$

$$\frac{1}{2}w\frac{d}{dw}[TIC] + \frac{d^2}{dw^2}(D_{TIC}[TIC]) = 0 \quad (19)$$

If the functions $[TAN](w)$and $[TIC](w)$ are solutions for Eqs. (18) and (19), then $[TAN]\left(\frac{z}{\sqrt{t}}\right)$and $[TIC]\left(\frac{z}{\sqrt{t}}\right)$ are solutions for Eqs. (15) and (16). Annex C presents the arguments for this conclusion.

It can be shown that for $[TAN](t, z)$ and $[TIC](t, z)$, both the initial conditions and infinite depth conditions are translated to the following, using the reduced variable w:

$$[TAN](w) \to [TAN]_\infty \text{ when } w \to \infty \quad (20)$$

$$[TIC](w) \to [TIC]_\infty \text{ when } w \to \infty \quad (21)$$

See Annex C for arguments.

Boundary conditions at the liquid–air interface

In the air transport can be described by Fick's second law $\frac{\partial f}{\partial t} = D\frac{\partial^2 f}{\partial z^2}$ (where $f =$ gaseous concentration of NH_3 or CO_2) and the solution to this equation is $f(w) = c_1 + c_2 erfc\left(\frac{w}{2\sqrt{D}}\right)$, using the reduced variable $w = \frac{z}{\sqrt{t}}$. Here c_1 and c_2 are arbitrary constants and $erfc(x)$ is the complementary error function defined by $erfc(x) = \frac{2}{\sqrt{\pi}}\int_x^\infty e^{-u^2}du$. Using $erfc(x) \to 0$ when $x \to \infty$, we see that c_1 is the concentration at infinity in air, i.e., the bulk value. Thus, for NH_3 we have:

$$[NH_3]_{Air}(t,z) = [NH_3]_{\infty,Air} + c_2 erfc\left(\frac{z}{2\sqrt{t}\sqrt{D_{NH_3,Air}}}\right) \quad (22)$$

This expression gives the correct initial condition and the boundary condition at infinite height.

Furthermore, the amount of NH_3 lost from the liquid at time t is $\int_0^\infty \left([TAN]_\infty - [TAN](t,z)\right)dz$. This is precisely the amount of NH_3 per unit area transferred from the liquid to air through the liquid–air interface during a period t.

The following transformations are made:

Ammonia transferred unit per area is:

$$\begin{aligned}&\int_0^\infty \left([TAN]_\infty - [TAN](t,z)\right)dz\\ &= \int_0^\infty \left([TAN]_\infty - [TAN](\tfrac{z}{\sqrt{t}})\right)dz\\ &= \sqrt{t}\int_0^\infty \left([TAN]_\infty - [TAN](w)\right)dw = \sqrt{t}F_{NH_3}\end{aligned}$$

The constant F_{NH_3} is defined as:

$$F_{NH_3} = \int_0^\infty \left([TAN]_\infty - [TAN]\right)dw \quad (23)$$

using the short form [TAN] for [TAN](w).

For the amount of NH_3 per unit area added to the air phase, the following transformations are made using Eq. (22):

$$\begin{aligned}&\int_0^\infty \left([NH_3]_{Air}(t,z) - [NH_3]_{\infty,Air}\right)\\ &= \int_0^\infty c_2 erfc\left(\frac{z}{2\sqrt{t}\sqrt{D_{NH_3,Air}}}\right)dz\\ &= 2\sqrt{t}\sqrt{D_{NH_3,Air}}c_2\int_0^\infty erfc(x)dx\\ &= \frac{2}{\sqrt{\pi}}\sqrt{t}\sqrt{D_{NH_3,Air}}c_2\end{aligned}$$

Using $\int_0^\infty erfc(x)dx = \frac{1}{\sqrt{\pi}}$

Therefore we must have $\sqrt{t}F_{NH_3} = \frac{2}{\sqrt{\pi}}\sqrt{t}\sqrt{D_{NH_3,Air}}c_2 \Leftrightarrow c_2 = \frac{\sqrt{\pi}F_{NH_3}}{2\sqrt{D_{NH_3,Air}}}$ and can express $[NH_3]$ in the air as:

$$[NH_3]_{Air} = [NH_3]_{\infty,Air} + \frac{\sqrt{\pi}F_{NH_3}}{2\sqrt{D_{NH_3,Air}}}erfc\left(\frac{w}{2\sqrt{D_{NH_3,Air}}}\right)$$

with $w = 0$ in this expression and using $erfc(0) = 1$, we find at the liquid–air boundary;

$$[NH_3]_{0,Air} = [NH_3]_{\infty,Air} + \frac{\sqrt{\pi}F_{NH_3}}{2\sqrt{D_{NH_3,Air}}} \quad (24)$$

Using similar arguments for [TIC], we obtain:

$$[CO_2]_{0,Air} = [CO_2]_{\infty,Air} + \frac{\sqrt{\pi}F_{CO_2}}{2\sqrt{D_{CO_2,Air}}} \quad (25)$$

$$F_{CO_2} = \int_0^\infty \left([TIC]_\infty - [TIC]\right)dw \quad (26)$$

We can then prove that knowledge of the total amount of NH_3 or CO_2 released from liquid to air gives important information about the concentrations of TAN and TIC species at the liquid–air interface. As a consequence of the differential equations [Eqs. (18) and (19)], the boundary conditions [Eqs. (20) and (21)], and Eqs. (23) and (26), then:

$$F_{NH_3} = 2\frac{d}{dw}(D_{TAN}[TAN])|_{w=0} \quad (27)$$

$$F_{CO_2} = 2\frac{d}{dw}(D_{TIC}[TIC])|_{w=0} \quad (28)$$

See Annex D for detailed arguments.

Henry's law demands that for all $t > 0$, $[NH_3]_0 = H_{NH_3}[NH_3]_{0,Air}$, and $[CO_2]_0 = H_{CO_2}[CO_2]_{0,Air}$ where H_{NH_3} and H_{CO_2} are the dimensionless Henry constants. Note that $z \to 0$ is equivalent to $w \to 0$. Using this, together with Eqs. (24), (25), (27) and (28), gives the two boundary conditions:

$$[NH_3]_0 = H_{NH_3}\left([NH_3]_{\infty,Air} + \sqrt{\frac{\pi}{D_{NH_3,Air}}}\frac{d}{dw}(D_{TAN}[TAN])|_{w=0}\right) \quad (29)$$

$$[CO_2]_0 = H_{CO_2}\left([CO_2]_{\infty,Air} + \sqrt{\frac{\pi}{D_{CO_2,Air}}}\frac{d}{dw}(D_{TIC}[TIC])|_{w=0}\right) \quad (30)$$

Observe that the flux of NH_3 from liquid to air at time t is:

$$\frac{\partial}{\partial t}\left(\sqrt{t}F_{NH_3}\right) = \frac{1}{2\sqrt{t}}F_{NH_3}$$

and that:

$$\begin{aligned}\frac{\partial}{\partial z}(D_{TAN}[TAN]) &= \frac{\partial}{\partial w}(D_{TAN}[TAN])\frac{\partial w}{\partial z} \\ &= \frac{1}{\sqrt{t}}\frac{\partial}{\partial w}(D_{TAN}[TAN])|_{w=0} \\ &= \frac{1}{\sqrt{t}}\frac{\partial}{\partial w}(D_{TAN}[TAN])|_{w=0} = \frac{1}{2\sqrt{t}}F_{NH_3}\end{aligned}$$

Therefore we obtain the equation $\frac{\partial}{\partial t}\left(\sqrt{t}F_{NH_3}\right) = \frac{\partial}{\partial z}(D_{TAN}[TAN])$, which resembles the conventional expression for the flux from liquid to air at the liquid–air interface.

The solution of the differential equations

The differential equations can be solved fully and effectively in the given situation. The outcome is predictions of the concentrations of all species in time and space, and the total transport of NH_3 and CO_2 from liquid to air at all times. To solve the two second-order differential Eqs. (18 and 19), it is necessary to have four conditions which are defined by the expressions in Eqs. (20), (21), (29) and (30). The differential Eqs. (18) and (19) with the conditions Eqs. (20), (21), (29) and (30) have exactly one solution. Therefore, making the substitution $w \to \frac{z}{\sqrt{t}}$ in that solution provides a solution to the original partial differential Eqs. (15) and (16), with the correct boundary conditions.

Our method of solution is based on the mathematical tool *Mathematica*. It is not our intention at this stage to find a method that is as effective as possible, but instead use a method which is very safe and fast enough to use here. In the solution, the values of all constants are first converted to exact numerical values so that they correspond to the original values with four significant digits. This avoids any rounding errors in intermediate algebraic results.

The problem in solving Eqs. (18) and (19) is that D_{TAN} and D_{TIC} are given as functions of $[H_3O^+]$ and only implicitly as functions of [TAN] and [TIC] through the equation, $Z_{total} = 0$. This problem was resolved as follows.

From $Z_{total} = 0$, we find [TIC] as an explicit algebraic expression depending on [TAN] and $[H_3O^+]$ alone. By replacing [TIC] in Eq. (19) with this expression, the original differential equations for [TAN] and [TIC] are transformed into two new coupled differential equations for [TAN] and $[H_3O^+]$. This is done automatically in *Mathematica* using exact algebra. Furthermore, these differential equations are solved in *Mathematica* using arbitrary precision to control round-off errors and the solutions are tested against the Eqs. (18)–(21), (29) and (30). With this model, concentrations for all species in time and space can be estimated in about 10 min.

Experimental

The model described above was evaluated with measured pH profiles in both time (0–20 h after stirring) and space (0–30 mm depth in the solution, with a depth resolution of 0.1 mm). Profiles of pH were measured in an 'ideal slurry solution' based on NH_4HCO_3, which includes the most important buffers for $[H_3O^+]$ in liquid animal slurry (Sommer and Husted 1995). The ideal slurry solution was composed of ammonium chloride (NH_4Cl, 0.05 M) and potassium bicarbonate ($KHCO_3$, 0.1 M) in MilliQ pure water, resulting in TAN and TIC concentrations of 0.05 and 0.1 M, respectively, and a bulk pH of 8.11 at 15.5 °C. As the model assumes instantaneous chemical equilibrium relative to diffusion, carbonic

Table 3 Conditions of the pH measurement experiments

Trial	*n*	Time (min)		Depth (mm)				Measured bulk pH
		Start	End	Start	End	Minimum	Maximum	
A1	15	1.0	8	1.48	0.08	0.08	1.48	8.11
A2	22	12	23	2.18	0.08	0.08	2.18	8.17
A3	52	26	53	5.17	0.07	0.07	5.17	8.16
A4	100	61	112	9.97	0.06	0.06	9.97	8.12
B1	15	1.1	8	1.46	0.06	0.06	1.46	8.19
B2	28	12	26	2.76	0.05	0.05	2.76	8.23
B3	52	29	55	5.15	0.05	0.05	5.15	8.23
B4	100	61	112	9.95	0.04	0.04	9.95	8.19
C1	15	1.1	8	1.44	0.04	0.04	1.44	8.24
C2	28	12	26	2.74	0.03	0.03	2.74	8.28
C3	52	30	56	5.13	0.03	0.03	5.13	8.27
C4	100	61	112	9.93	0.02	0.02	9.93	8.26
C5	219	180	293	21.91	0.08	0.08	21.91	
C6	219	300	413	21.88	0.06	0.06	21.88	
C7	219	420	533	21.86	0.04	0.04	21.86	
C8	219	540	653	21.84	0.02	0.02	21.84	
C9	219	660	773	21.82	0.00	0.00	21.82	
C10	218	780	893	21.8	0.08	0.08	21.8	
C11	218	900	1,013	21.78	0.06	0.06	21.78	
C12	218	1,020	1,133	21.75	0.03	0.03	21.75	
C13	23	1,194	1,207	31.22	1.72	1.72	31.22	8.24

In the trial column, the letter (A, B, or C) indicates the set

anhydrase (Novozyme carbonic anhydrase NZSBM01, 70,000 Wilbur-Anderson units (WAU) per mL) was added to the solution (60 mL/L) to minimise the effect of a slow hydration/dehydration rate of H_2CO_3. An 850 mL portion of this 'ideal slurry solution' was transferred to a rectangular glass beaker (177 mm long, 50 mm width, 125 mm high), corresponding to a filling height of 96 mm.

The study was carried out in a thermostatically controlled room set at an air temperature of 15.5 °C, and all liquids were acclimatised by storage in airtight containers in the room for at least 24 h prior to the experiment. To ensure constant temperature and humidity, all measurements were conducted inside a 60 cm × 60 cm × 60 cm aluminium chamber coated with about 1 cm of expanded polystyrene for insulation. The chamber was kept closed during the entire experiment. Evaporation from the solution was minimised by a constant high relative air humidity of 85 % inside the chamber, maintained by a box of water with a cotton wick. Relative air humidity and temperature inside the polyethylene box were monitored every minute during the experiment using a HumidiProbe (PicoTechnology, Cambridgeshire, United Kingdom), and bulk solution temperature was monitored every minute with a Thermocouple datalogger EL-USB-TC-LCD (Lascar Electronics UK, Salisbury, United Kingdom). The rate of evaporation was measured as the reduction in water level at the end of the experiment, and was measured with a precision of 20 μm, by aligning a microsensor to the surface (see below). The acclimatised solution was transferred to the glass beaker and measurements were started when the air temperature and relative humidity were constant. At this time, the solution was stirred without opening the chamber using a magnet stirrer that was activated from outside the chamber. Termination of stirring defined the start of a series of measurements, i.e., time zero. At the end of a measurement series the liquid was stirred with the magnet without opening the box, and the time of stirring termination started a new series. The experiment was repeated three times with at least four complete pH and temperature profiles measured during each series, (Table 3). We refer to

Table 4 Summary of model fit for series A and B

Trial	Maximum measured pH				Mean absolute error	Mean bias	RMSE	Pearson's r	Slope
	Measured	Calculated	Depth (mm)	Time (min)					
A1	9.12	9.10	0.08	8	0.016	−0.0031	0.019	0.999	0.978
A2	9.23	9.12	0.08	23	0.069	−0.069	0.075	0.995	0.962
A3	9.27	9.13	0.07	53	0.085	−0.085	0.090	0.997	1.02
A4	9.29	9.14	0.06	112	0.078	−0.078	0.088	0.998	1.09
B1	9.10	9.12	0.06	8	0.035	0.024	0.040	0.998	0.933
B2	9.19	9.14	0.05	26	0.026	−0.026	0.035	0.998	0.972
B3	9.23	9.14	0.05	55	0.057	−0.057	0.060	0.998	1.00
B4	9.28	9.15	0.04	112	0.065	−0.065	0.072	0.997	1.06

Depth and time in the "Maximum measured pH" section refer to the location and time of the maximum measured pH. The calculated value is from the same time and location. RMSE = root mean square error. Mean absolute error, bias, and RMSE are all in pH units

each complete profile measurement as a "trial" and each set of trials a "series", of which there were three—series A, B, and C. Temperature and pH were monitored vertically with a depth resolution of 0.1 mm, between 0 and 10 mm depth (increasing depth for each consecutive trial) during the first 2 h after stirring. In series C, trials continued every 2 h for an additional 18 h to a total depth of 31 mm. In each trial pH was measured from below with a modified microsensor to avoid disturbance of the liquid surface (Markfoged 2013). Since series A, B, and C were performed on the same liquid, but with stirring in between, the bulk concentration of the buffers changed during the experimental period and resulted in a small increase in the bulk pH (0.2 pH units) during the entire experiment (Table 3). The initial TIC and TAN concentrations used for model predictions for series B were calculated by subtracting predicted cumulative emission from the concentrations at the start of series A for this effect. Model predictions with air diffusion coefficients multiplied by 4.0 were used to make these predictions, as described below.

Temperature profiles were conducted with a thermocouple copper/constantan T-type microsensor connected to a T301 thermocouple meter. Profiles of pH was conducted with a pH microelectrode (Revsbech and Jorgensen 1986) connected to a reference electrode (Radiometer, Lyon, France) and to a mV meter (Unisense A/S, Aarhus, Denmark). The pH-sensitive end of the electrode was 0.2 mm long, and was bent to be horizontal (parallel to the solution surface) to maximize spatial resolution. Both the temperature sensor and the pH electrode were bent to form a hook so measurements could be made from below the surface even though the main body of the electrode entered the solution from above. This eliminated the problem of a meniscus forming for measurements near the surface when measuring from above (Markfoged 2013). These modifications provided a maximum spatial resolution of 20 μm. The system had a resolution in pH measurements of 0.01 units. The electrode was calibrated using three buffers (pH 6.865, 7.413, and 9.180) at the same temperature as the solution. Drift in of the pH response was <0.02 pH units from the beginning to end of the experiment. The software SensorTrace Pro (Unisense A/S, Aarhus Denmark) was used to control the position of the sensors and to store the digitised sensor signal. Prior to the experiments, all sensor tips were depth-aligned to the liquid surface within 20 μm. Additional details on measuring pH and temperature can be found in Markfoged (2013).

Two approaches were used to quantitatively evaluate model fit. Since the magnitude of pH increase is important, we compared maximum measured pH to the calculated value at the same time and location for each trial. According to the model there is a single maximum pH for all t (its value is the limiting pH as $w \rightarrow 0$). However, since this value occurs only as $z \rightarrow 0$, measured values will always be lower than this value, since measurement requires a finite volume. Also, we used five measures of model fit to summarize fit over all points in each evaluation trial: mean absolute error, mean bias, root mean square error (RMSE), least-squares slope (calculated versus measured), and Pearson's correlation coefficient. Only

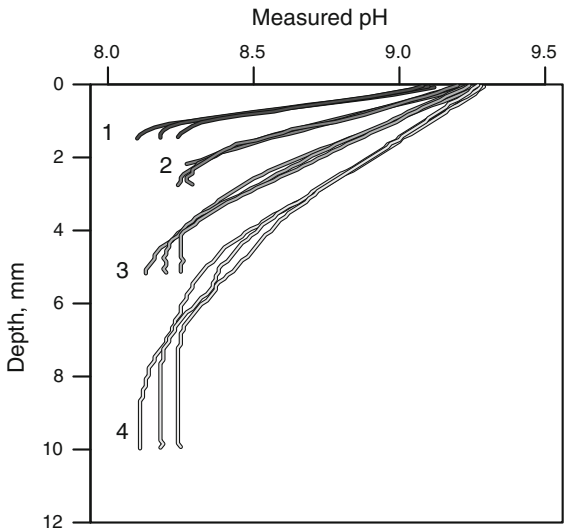

Fig. 2 Measured pH for the three series (A, B and C) during time intervals 1 (1–8 min), 2 (about 12–25 min), 3 (about 30–60 min), and 4 (60–110 min). Note that the measured pH profiles cannot be used for gradient calculations, as the processes are not steady-state during the timespan of a profile. See Tables 3 and 4 for details on the trials

series A and B were used for model evaluation; series C was excluded because of accumulated uncertainty in initial TAN and TIC concentrations due to emission during series A and B and the longer trials, which mean more deviation from model assumptions. We found that bulk pH calculated by the model was about 0.03 units lower than measured values, possibly to due to omission of activity corrections (i.e., effects of long-range ion interactions on deviations from ideal behaviour in the calculation of species concentrations) in the model. Therefore, 0.03 was added to all calculated values of pH.

Results and discussion

Measurements of air and liquid temperature, relative air humidity and liquid evaporation rate showed that convective transport in the liquid was very limited. The air temperature varied by <0.45 °C in series A and B and by 0.4–2.5 °C in series C, and the relative humidity was always above 87 %. The liquid temperature from the air–liquid interface to a depth of 31 mm varied by less than 0.4 °C, with no indication of a gradient near the surface. In addition, the average water evaporation rate from the solution was only 0.179 μm min^{-1}. The constant temperature over time and depth in the ideal slurry solution, the rapid formation of a gradient in pH (indicating underlying gradients in solute concentrations), and the similarity of pH profiles measured at different times (when plotted versus the reduced variable w) strongly suggest that convective transport in liquid was not significant. While it is unrealistic to assume that movement of water immediately ceased when stirring stopped, there is no evidence that it continued for long and contributed to convective transport. Therefore the profile data seem appropriate for evaluating the mathematical model, which assumes that buffer species are transported only by diffusion to the surface of the liquid.

Measurement of pH in all three series (A, B, and C) showed an increase in pH, initially close to the surface (Fig. 2). Over time, the resulting pH gradient migrated downward, with a measureable increase in pH reaching a depth of about 10 mm after 2 h, about 15 mm after 5 h, and >30 mm after 20 h (Figs. 3, 4). Measurements made over a longer period in series C shows that the pH changed for at least 16 h (Fig. 3). From the perspective of a fixed location, measurements showed a gradual increase in pH over time.

The pH near the surface increased from 8.2 to 9.15 during 10 min of exposure of the liquid to the atmosphere, to a maximum of 9.46 after approximately 20 h of exposure (Figs. 3, 4). It is important to note that for each profile, the pH was measured over a time period of 5.5 min per mm of depth moved, and that the pH during measurement of a profile changed with time, so these profiles (Figs. 3, 4) do not represent the condition at a single point in time and cannot be used directly in mass transfer calculations. The magnitude of the increase in pH is similar to the increase in the near-surface pH (0–1 mm) of a thin layer of slurry (Sommer and Sherlock 1996) and of stored pig slurry (Canh et al., 1998). The difference between the profiles was larger in the series measured up to 13 h soon after stirring than from 13 to 19 h, where the profiles of different time series are very similar, indicating that the change in composition slowed over time (Fig. 4).

Use of the reduced variable $w = \frac{z}{\sqrt{t}}$ in our model implies that pH is not dependent on time per se, but instead pH versus z profiles at different times are simply one single profile stretched out over z as time proceeds. If this is correct, pH profiles from different

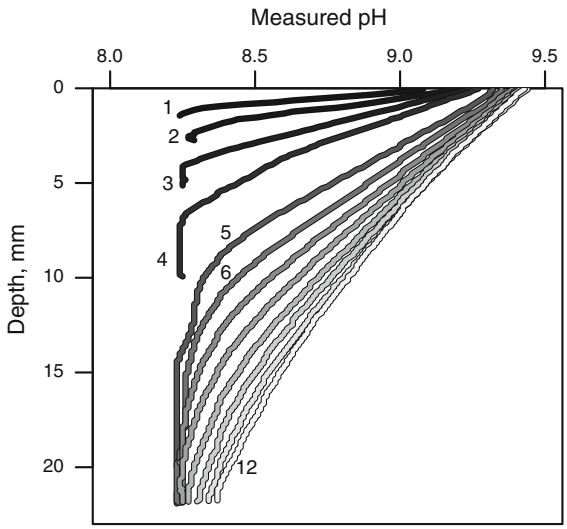

Fig. 3 Measured pH profiles from series C trials 1 through 12. Dark lines are from earlier times and lighter lines later. Numeric labels identify individual trials within the C series. Trial C13 plots over trial C12 and is not shown here. Note that the profiles cannot be used for gradient calculations, as the processes are not steady-state during the timespan of a trial

time periods will converge to a single curve when plotted versus w. Results from series A suggest that this is true (Fig. 4). Another implication of the reduced variable w is that the migration of a particular pH value downward is proportional to $\sqrt{t}$. So on a plot of z versus $\sqrt{t}$, lines of constant pH will have a constant negative slope and an intercept of zero. Results from the C series shows that this response (constant negative slope and intercept near zero) is present, with some variability (Fig. 4). Together these results provide strong support for the introduction of the reduced variable w, which is an important contribution of this work, because it simplifies the calculations needed for making predictions, and can reduce computational time required for a solution.

In general, the pH predictions from the model agreed with the measured values in series A and B, although differences increased at later times and deeper locations, especially for series A (Fig. 6). The mean absolute error, mean bias, and RMSE were <0.05 pH units for trials A1, B1, and B2 and were <0.1 for all trials used for model evaluation (Table 4). Calculated maximum pH was within 0.15 units of measured values for all evaluation trials. Considering that measured pH changed by >1.1 in individual trials, this appears to be a good fit. Correlation between measured and calculated pH was very high (>0.994) and all slopes of calculated versus measured pH were within 6 % of unity (Table 4). Together, these results strongly suggest that the basic structure of the model and the expressions used for assessing equilibrium reactions and diffusion are appropriate.

Some of the differences between measured and calculated results at later times are likely due to limitations of the experimental setup in matching the

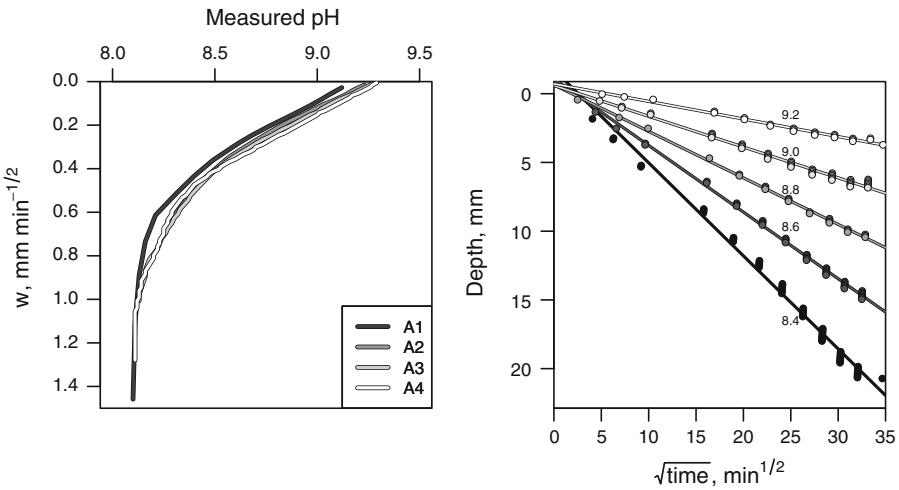

Fig. 4 Measured pH versus the reduced variable w (*left*). The position on the y (w) axis can be interpreted as the depth in mm after 1 min or the depth in cm after 1 h and 40 min. Locations and times of constant measured pH values from all trials in series C (*right*). Measured pH was taken as equaling the specified value if it was within 0.01 pH units (i.e., points labeled 8.4 may range from 8.39 to 8.41). Lines show least-squares linear models for each series of transformed points

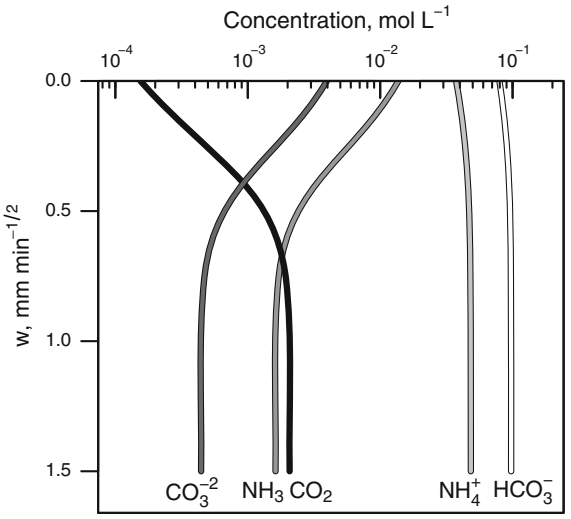

Fig. 5 Calculated concentrations of TAN and TIC species for the default scenario

model, which assumes vertical transport only. The edge of the glass chamber was 3.0 cm above the liquid surface and gas transport within this volume is only vertical. Above the edge, the gas will be transported both horizontally and vertically, and consequently the transport rate may be higher later in the emission event. Increasing the magnitude of diffusion coefficients in air slightly improved model fit at later times. Multiplication of diffusion coefficients by a factor of 4.0 seemed to result in the best fit to the trials started after 10 min (A2–A4) (Fig. 6) (out of all integers between one and ten).

The model calculations show that species concentrations are greatly affected by emissions of CO_2 and NH_3 (Fig. 5). At all depths, HCO_3^- was by far the most important species of TIC at the pH values in this solution: at least 40 times the concentration of CO_3^{2-} and CO_2. Therefore, HCO_3^- is responsible for most of the transport of TIC to the surface. The concentration of H_3O^+ decreased towards the surface (pH increased), while the concentration of NH_3 increased and that of NH_4^+ decreased. With HCO_3^- dominating TIC transport, the effect of including variable diffusion coefficients is relatively small. On the other hand, if species concentration differs from those given in the system described, it may result in erroneous calculations to only use one diffusion coefficient for all species. One case where differences in diffusion coefficients would likely be more important is slurry that has been acidified to a pH below 6 (as used in the technology presented by Kai et al. (2008)), where the concentrations of CO_2 and H_2CO_3 become more important. However, the independent diffusion of all species used in our model is also a simplification.

Sensitivity analysis was used to assess the importance of gas-phase and liquid-phase transport limitation, and the impact of liquid diffusion coefficients. Assuming a single diffusion coefficient value for all species slightly reduced the accuracy of the model, especially at small w (Fig. 6, line 3). The effect on emission was small and positive for NH_3, but larger and negative for CO_2 (Fig. 7, line 3). Apparently transport through both the solution and air limit emission, although possibly in opposite directions for NH_3 and CO_2. Multiplication of diffusion coefficients in air for both NH_3 and CO_2 by 4.0 increases the pH at low values of w (i.e., at small z or large t) and has a smaller effect at large values of w (Fig. 7, line 4). This change more than doubles NH_3 emission, but only slightly increases CO_2 emission. Reducing diffusion coefficients for aqueous species also causes an increase in pH for small w, but reduces pH at moderate values of w, i.e., for a fixed t, this change reduces the depth to which a given pH value penetrates (Fig. 7, line 4). Effects on emission are smaller, and opposite in sign for NH_3 and CO_2 (Fig. 7, line 4). An important conclusion from this analysis is that similar pH profiles (Fig. 7 top, lines 1 and 2) can result from scenarios that produce very different emissions (Fig. 7 middle, lines 1 and 2). Therefore, future evaluation should include both pH and emission measurements.

The pH in relation to depth and time, and rates of NH_3 and CO_2 emission are the result of a large number of processes and interactions of processes, which is the reason a complex model is needed for the calculation. At the same time one can't explain the results as the outcome of one or few processes. Changing the transfer in the air phase from diffusion-limited to unlimited changes the species profile significantly. For example, NH_3 increases towards the surface when air diffusion is included whereas the maximum NH_3 is seen below the surface with unlimited transport in the air phase. The reason for this difference is that H_3O^+ is less in the surface layers and TAN relatively greater, while in lower layers H_3O^+ was greater and thus NH_3 is lower. In this environment, HCO_3^- declined significantly towards the surface and CO_3^{2-} increased.

Simplifications made in the development of our model do not appear to substantially affect its

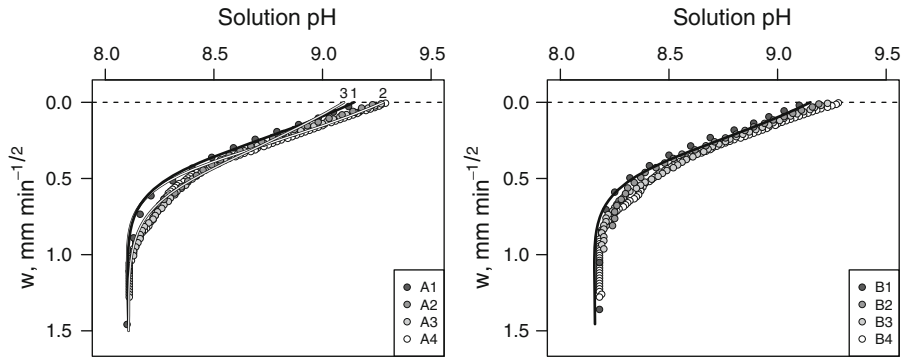

Fig. 6 Measured (*points*) and calculated (*lines*) pH profiles for series A (*left*) and B (*right*) for scenarios (1) default, (2) air diffusion coefficients multiplied by 4.0, and (3) all solution diffusion coefficients for all species set to a constant value (1.23×10^{-5} cm^2 s^{-1})

accuracy. Specifically, all computations were carried out using species concentrations and not activities, and all aqueous species diffuse independently of each other in our model. Despite these simplifications, calculated pH values were close to measured values (Fig. 6). Regardless, future work should address the significance of these simplifications. For animal slurry, other processes may influence NH_3 emission in addition to the chemical and physical processes considered here. For example, sorption of ions to organic matter can reduce concentrations of cations in solution, and microbial activity can affect pH through generation of CO_2 and organic acids. Additionally, convective transport of slurry solutes may occur. For slurry with a high dry matter content, convection is probably not important, but for slurry with a low dry matter content, or stored slurry, this may not be the case. Although these processes may influence the exact changes in pH over time and depth, it is likely that the effects described in this work will still exist in slurry.

Our model makes predictions that are important to consider in measurement studies. First, at any time greater than 0, the pH closest to the surface (as z and $w \rightarrow 0$) is constant, although initially it increases over a very small distance, and the increase in pH would be impossible to measure. The definition of "surface" is important. Additionally, predicted fluxes of NH_3 and CO_2 are predicted to start at a maximum value and always decline. Conversely, the model developed by Hafner et al. (2013) predicted an initial increase in NH_3 flux as surface pH increased. Whether this increase is an inaccuracy inherent in the numerical approach used or an actual physical phenomenon could be determined by experimental work.

The results from this study could contribute to the development of simple black box models with little need of information for decision support when assessing the emission of NH_3 from stored slurry or slurry applied to soils. This approach could contribute to improve a number of models that currently do not include pH (Zimmo et al. 2003; McLaughlin et al. 2012). For example, emission from two pig slurries, with the same TAN and pH, but one having a higher TIC concentration (due, perhaps, to storage or anaerobic digestion) would emit different amounts of NH_3 over a given time period. The model presented here could predict this effect, while existing models used for predicting emission from field-applied slurry could not.

Conclusions

Here we have used high-resolution pH measurements and a new mathematical model to provide the most detailed exploration to date of interactions between NH_3 and CO_2 emission and surface pH in a NH_4HCO_3 solution. The qualitative and quantitative match between measured and calculated pH profiles suggests that our model, and the relationships used for calculating equilibrium and Henry's law constants, are accurate. This evaluation is an important new contribution of our work. Furthermore, new developments in our model—the combination of time and location into a single variable, and the analytical solution developed using *Mathematica*—should facilitate future work on this topic by making model calculations easier, and providing insights into how pH gradients change over time and space. The application of these results and

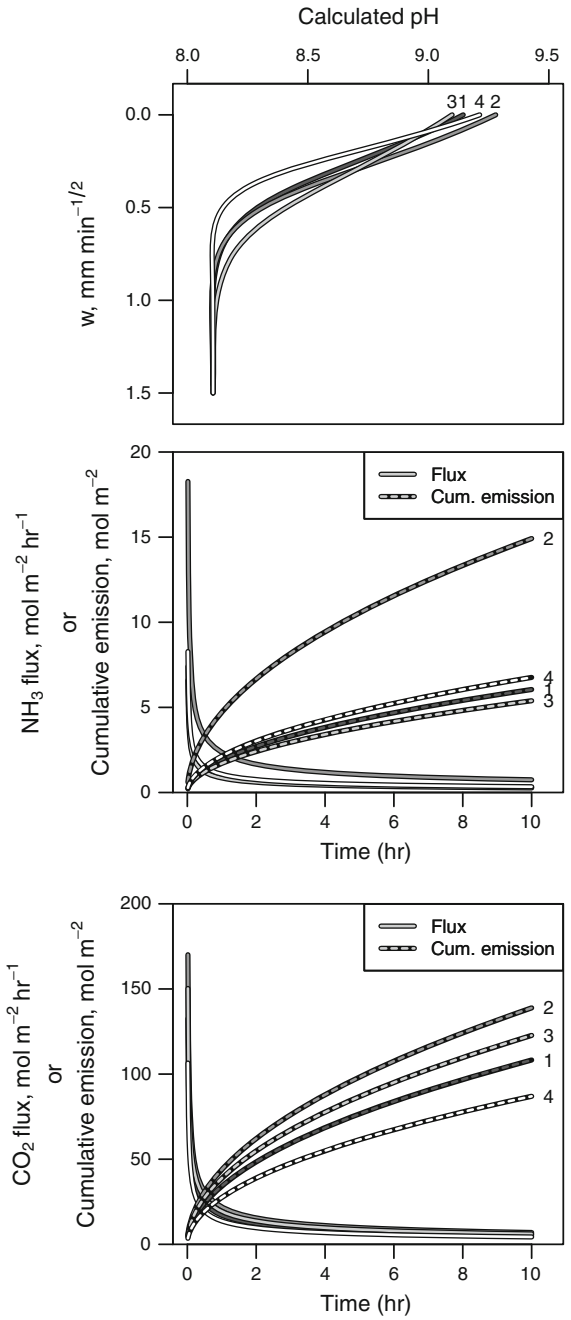

Fig. 7 Calculated pH and NH_3 and CO_2 emission for four scenarios: (1) default scenario, (2) air diffusion coefficients multiplied by 4.0, (3) all solution diffusion coefficients for all species set to a constant value (1.23×10^{-5} cm^2 s^{-1}), and (4) all water diffusion coefficients divided by 2.0

our model to NH_3 emission from dairy slurry, which can be thought of as an NH_4HCO_3 solution with additional solutes and particulate material, is clear. Future modelling and measurement work is needed to quantify these effects in actual field-applied slurry. Future modelling work should include effects of activity corrections, effects of kinetically limited reactions, interactions in diffusion, extension to finite depths, and evaluation of the importance of convection.

Acknowledgments We thank Grønt udviklings- og demonstration program for the financial support (Gylle—IT), Ministeriet for Fødevarer, Landbrug og Fiskeri - NaturErhvervstyrelsen. We thank Lars B Pedersen, Preben Sørensen, and and Niels Peter Revsbech (Aarhus University, Bioscence - European Research Council, Grant No. 267233) for constructing the hock formed temperature sensors and pH electrodes, Steen Bennike Mortensen (NovoZymes) for providing us with the carbonic anhydrase and Henrik Midtiby for valuable comments to the model development.

References

Beusen AHW, Bouwman AF, Heuberger PSC, Van Drecht G, Van Der Hoek KW (2008) Bottom-up uncertainty estimates of global ammonia emissions from global agricultural production systems. Atmos Environ 42:6067–6077

Beutier D, Renon H (1978) Representation of NH3-H2S-H2O, NH3-CO2-H2O, and NH3-SO2-H2O vapor-liquid equilibria. Ind Eng Chem Process 17:220–230

Blanes-Vidal V, Sommer SG, Nadimi ES (2009) Modeling surface pH and emissions of hydrogen sulphide, ammonia, acetic acid and carbon dioxide from a swine waste lagoon. Biosyst Eng 104:510–521

Broboff S, Phillips RJ, Shekarriz A (1998) Nuclear magnetic resonance measurement of ammonia diffusion in dense solid–liquid slurries. Pacific Northwest National Laboratory Richland, Washington. PNNL-11678 (REV.1 UC-2030. pp 25

Buijsman E, Maas JF, Asman WAH (1987) Anthropogenic NH_3 emissions in Europe. Atmos Environ 21:1009–1022

Bussink DW, Huijsmans JFM, Ketelaars JJMH (1994) Ammonia volatilization from nitric-acid-treated cattle slurry surface applied to grassland. Neth J Agric Sci 42:293–309

Canh TT, Sutton AL, Aarnink AJA, Verstegen MWA, Schrama JW, Bakker GCM (1998) Dietary carbohydrates alter the fecal composition and pH and the ammonia emission from slurry of growing pigs. J Anim Sci 76:1887–1895

Chaoui H, Montes F, Rotz CA, Richard TL (2009) Volatile ammonia fraction and flux from thin layers of buffered ammonium solution and dairy cattle manure. Trans ASABE 52:1695–1706

Davidson EA (2009) The contribution of manure and fertilizer nitrogen to atmospheric nitrous oxide since 1860. Nat Geosci 2:659–662

EU (2001) Directive 2001/81/EC of the European Parliament and of the Council. On national emission ceilings for certain atmospheric pollutants. Official Journal of the European Communities. L 309/22 to L 309/30

Frank MJW, Kuipers JAM, van Swaaij WPM (1996) Diffusion coefficients and viscosities of $CO_2 + H_2O$, $CO_2 + CH_3OH$, $NH_3 + H_2O$, and $NH_3 + CH_3OH$ liquid mixtures. J Chem Eng Data 41:297–302

Galloway J, Aber J, Erisman J, Seitzinger S, Howarth R, Cowling E, Cosby B (2003) The nitrogen cascade. Bioscience 53:341–356

Génermont S, Cellier P (1997) A mechanistic model for estimating ammonia volatilisation from slurry applied to bare soil. Agric For Meteorol 88:145–167

Hafner SD, Bisogni JJ (2009) Modeling of ammonia speciation in anaerobic digesters. Water Res 43:4105–4114

Hafner SH, Montes F, Rotz CA (2013) The role of carbon dioxide in emission of ammonia from manure. Atmos Environ 66:63–71

Hutchings NJ, Sommer SG, Andersen JM, Asman WAH (2001) A detailed ammonia emission inventory for Denmark. Atmos Environ 35:1959–1968

Kai P, Pedersen P, Jensen JE, Hansen MN, Sommer SG (2008) A whole-farm assessment of the efficacy of slurry acidification in reducing ammonia emissions. Eur J Agron 28:148–154

Kerstin J, Sokolov M, Wakeham WA (1978) Viscosity of liquid water in the range -8 °C to 150 °C. J Phys Chem Ref Data 7:941–948

Markfoged M (2013) Microbial control of gas-exchange at air–manure interfaces. PhD thesis, University of Aarhus, Aarhus

Marrero TR, Mason EA (1972) Gaseous diffusion coefficient. J Phys Chem Ref Data 1:1–117

McLaughlin MR, Brooks JP, Adeli A (2012) Temporal flux and spatial dynamics of nutrients, fecal indicators, and zoonotic pathogens in anaerobic swine manure lagoon water. Water Res 46:4949–4960

Ni J (1999) Mechanistic model of ammonia release from liquid manure: a review. J Agric Eng Res 72:1–17

Revsbech NP, Jorgensen BB (1986) Microelectrodes—their use in microbial ecology. Adv Microbiol Ecol 9:293–352

Sommer SG, Husted S (1995) A simple model of pH in slurry. J Agric Sci 124:447–453

Sommer SG, Sherlock RR (1996) pH and buffer component dynamics in the surface layers of animal slurries. J Agric Sci 127:109–116

Spiller LL (1989) Determination of ammonia/air diffusion coefficient using nafion lined tube. Anal Lett 22:2561–2573

Sutton MA, Oenema O, Erisman JW, Leip A, van Grinsven H, Winiwarter W (2011) Too much of a good thing. Nature 472:159–161

United Nations (2004) Handbook for the 1979 convention of long-range transboundary air pollution and its protocols. UNECE Publication Unit, Geneva, Switzerland. http://www.unece.org/env/lrtap/BIBLE.E.pdf

Van der Molen J, Beljaars ACM, Chardon WJ, Jury WA, Van Faassen HG (1990) Ammonia volatilization from arable land after application of cattle slurry. 2. Derivation of a transfer model. Neth J Agric Sci 38:239–254

Zeebe RE (2011) On the molecular diffusion coefficients of dissolved CO_2, HCO_3^-, and CO_3^{2-} and their dependence on isotopic mass. Geochim Cosmochim Acta 75:2483–2498

Zimmo OR, van der Steen NP, Gijzen HJ (2003) Comparison of ammonia volatilisation rates in algae and duckweed-based waste stabilisation ponds treating domestic wastewater. Water Res 37:4587–4594